Asian Journal of Pharmaceutical Sciences 16 (2021) 363–373

Available online at www.sciencedirect.com

ScienceDirect

journal homepage: www.elsevier.com/locate/AJPS

Original Research Paper

# pH-sensitive micelles self-assembled from star-shaped TPGS copolymers with ortho ester linkages for enhanced MDR reversal and chemotherapy

*Yong Xu*[1], *Shi Wang*[1], *Longshun Yang*, *Yuhang Dong*, *Yafang Zhang*, *Guoqing Yan*[*], *Rupei Tang*[*]

*Engineering Research Center for Biomedical Materials, Anhui Key Laboratory of Modern Biomanufacturing, School of Life Sciences, Anhui University, Hefei 230601, China*

ARTICLE INFO

*Article history:*
Received 25 August 2020
Revised 27 January 2021
Accepted 29 January 2021
Available online 25 February 2021

*Keywords:*
TPGS
Ortho esters
Star-shaped copolymers
MDR reversal

ABSTRACT

TPGS approved by FDA can be used as a P-gp inhibitor to effectively reverse multi-drug resistance (MDR) and as an anticancer agent for synergistic antitumor effects. However, the comparatively high critical micelle concentration (CMC), low drug loading (DL) and poor tumor target limit its further clinical application. To overcome these drawbacks, the pH-sensitive star-shaped TPGS copolymers were successfully constructed via using pentaerythritol as the initial materials, ortho esters as the pH-triggered linkages and TPGS active-ester as the terminated MDR material. The amphiphilic star-shaped TPGS copolymers could self-assemble into free and doxorubicin (DOX)-loaded micelles at neutral aqueous solutions. The micelles exhibited the lower CMC ($8.2 \times 10^{-5}$ mg/ml), higher DL (10.8%) and long-term storage and circulation stability, and showed enhanced cellular uptake, apoptosis, cytotoxicity, and growth inhibition for *in vitro* MCF-7/ADR and/or MCF-7/ADR multicellular spheroids and *in vivo* MCF-7/ADR tumors via efficiently targeted drug release at tumoral intracellular pH (5.0), MDR reversal of TPGS, and synergistic effect of DOX and TPGS. Therefore, the pH-sensitive micelles self-assembled from star-shaped TPGS copolymers with ortho ester linkages are potentially useful to clinically transform for enhanced MDR cancer treatment.



## 1. Introduction

Multi-drug resistance (MDR) remains a serious phenomenon to restrict the successful chemotherapeutic treatment, and this phenomenon exists in nearly every clinic drug, even the latest agents [1–6]. MDR involves various mechanisms and the drug efflux mediated by ATP-binding P-glycoprotein (P-gp) is one of the most investigated and characterized mechanisms [3,7–10]. Vitamin E d-α-tocopheryl

* Corresponding authors.
*E-mail addresses:* 17017@ahu.edu.cn (G.Q. Yan), tangrp99@iccas.ac.cn (R.P. Tang).
[1] Both the authors contributed equally to this work.
Peer review under responsibility of Shenyang Pharmaceutical University.

https://doi.org/10.1016/j.ajps.2021.01.002

poly(ethylene glycol) 1000 succinate (TPGS) approved by FDA as a P-gp inhibitor, can effectively reverse MDR via the depletion of intracellular ATP and inhibition of substrate induced ATPase activity [11–14]. Moreover, TPGS can be applied as an anticancer agent for synergistic antitumor effects through ROS generation, downregulation of anti-apoptotic proteins and DNA damage [15]. However, TPGS-based micelles exhibit the comparatively high critical micelle concentration (CMC), low drug loading (DL) and poor tumor target, suggesting unstable blood circulation and poor chemotherapy efficiency [16–19]. To overcome these drawbacks, it is urgent to optimize the structure of TPGS to fabricate a preferred drug delivery system for enhanced MDR reversal and cancer therapy.

The amphiphilic TPGS (1500 Da) with a hydrophile/lipophile balance (HLB) value of 13.2, is composed of single vitamin E succinate and poly(ethylene glycol) (PEG) 1000 [13]. Its low molecular weight and short hydrophilic and hydrophobic part give rise to the high CMC and low DL of TPGS-based micelles, due to the weak intermolecular interaction forces between TPGS or between TPGS and hydrophobic drugs [16,17]. To improve these physical properties, it is necessary to optimize the structure of TPGS for enhancement on intermolecular interaction forces [16,20,21]. On one hand, lots of TPGS-based nano-prodrugs such as TPGS-gemcitabine, TPGS-mitoxantrone and TPGS-doxorubicin (DOX) can improve the DL, but the CMC is still at a high level [22–24]. On the other hand, TPGS-based polymeric or mixed micelles may flexibly regulate the micellar CMC and DL by means of specific polymer structures, but the low content of TPGS in the copolymers weakens the ability to reverse MDR and promote apoptosis [25–27]. Thus, there has been great interest to design a special TPGS-based drug delivery system for both of low CMC, and high DL and TPGS content. The nano-carriers self-assembled from amphiphilic star-shaped copolymers have been recently paid much attention, because of their special physicochemical properties like lower CMC, and higher DL and encapsulation efficiency (EE) than the linear copolymers with identical molecular masses [28–31]. Therefore, star-shaped TPGS copolymers may have great potential to overcome the above drawbacks via conjugating multiple TPGS with a specific multi-arm group. The star-shaped TPGS copolymers may enhance intermolecular hydrophobic interaction, $\pi$-$\pi$ stocking, hydrogen bonding and van der Waals force between branched vitamin E succinate each other or/and hydrophobic chemotherapy drugs, for decreased CMC and increased DL while maintaining the high TPGS content, in comparison with TPGS-based micelles [20,21,29–31]. Additionally, the terminal hydroxyl group of PEG in TPGS is an active functional group, which can easily conjugate with the specific multi-arm group by further modification. Notably, to simultaneously achieve tumor targeting capability, the key problem is how to construct such a functional multi-arm group.

The hypoxia at tumor tissues leads to an evidently acidic gradient distribution from blood vessels (pH = ~7.4) to tumor cells (pH = ~4.0–6.0) [32–35]. It is a desirable strategy to construct an intracellular pH-sensitive multi-arm group to conjugate TPGS for targeted release of the embedded drug and TPGS. Ortho esters, whose hydrolysis rate might improve 1–4 orders of magnitude in response to mildly acidic condition compared to other acid labile linkages such as esters, hydrazines and acetals, have great potential to construct such an intracellular pH-triggered multi-arm group [36–38]. Pentaerythritol containing four hydroxyl groups has been widely used in surfactants and pharmaceutical materials [31,39], and could sequentially react with ortho ester linkages reported in our previous literatures [40,41], and TPGS to fabricate such star-shaped TPGS copolymers, which could further self-assemble into pH-sensitive drug-loaded micelles with low CMC, high DL and enhanced MDR reversal and targeted cancer treatment (Scheme 1).

## 2. Materials and methods

### 2.1. Materials

Dichloromethane (DCM) was dehydrated over $CaH_2$ before use. Vitamin E d-α-tocopheryl poly(ethylene glycol) 1000 succinate (TPGS, TCI), di(N-succinimidyl) carbonate (DSC, 98%, TCI), pyridinium p-toluenesulfonate (Py-pTSA, 98%, Aladdin), doxorubicin hydrochloride (DOX•HCl, 98%, Aladdin), pentaerythritol (99%, Macklin) and 3-(4,5-dimethylthiazol-2-yl)−2,5-diphenyltetrazolium bromide (MTT, 98%, Macklin) were used without further purification. 2,2,2-trifluoro-N-((2-methoxy-1,3-dioxolan-4-yl)methyl)acetamide (TA) was prepared according to the previous literature [41]. Alexa fluor® 488 annexin V/dead cell apoptosis assay kit, ATP assay kit and ROS assay kit were obtained from Beyotime Biotechnology Co.,Ltd. (Nantong, China). The human breast cancer cell line (MCF-7) and DOX-resistant breast cancer cell line (MCF-7/ADR) were purchased from American Type Culture Collection (ATCC). Female BALB/c nude mice at the age of 5–6 weeks were purchased from the Cavens Laboratory Animal Limited Company (Changzhou, China) and used in the Guide of Experimental Animal Ethics Committee of Anhui University.

### 2.2. Synthesis of TPGS-active ester

In a nitrogen atmosphere, triethylamine (TEA, 2.76 ml, 2.02 g) was slowly dropped into the mixture of TPGS (15.1 g), DSC (20.0 mmol, 5.12 g) and DCM (125 ml) for 0.5 h under the ice bath, and continuously stirred for another 12 h. The crude product was evaporated by rotary evaporator and precipitated in anhydrous diethyl ether for three times. Finally, the product (15.0 g, 91.5%) was yielded via vacuum distillation and determined by $^1$H Nuclear Magnetic Resonance (NMR).

### 2.3. Synthesis of fluorinated star-shaped ortho esters (FPOE)

The mixture of pentaerythrotol (10.0 mmol, 1.36 g), TA (80.0 mmol, 18.33 g) and Py-pTSA (0.8 mmol, 0.15 g) reacted at 125 °C for 6 h under vacuum distillation, and was dissolved in ethanol (30 ml) when cooled to room temperature. Afterwards, the solution was dialyzed (500 Da) against ethanol for 48 h. Finally, the product (6.9 g, 75.0%) was obtained by vacuum distillation and determined by $^1$H NMR and mass spectrometer.

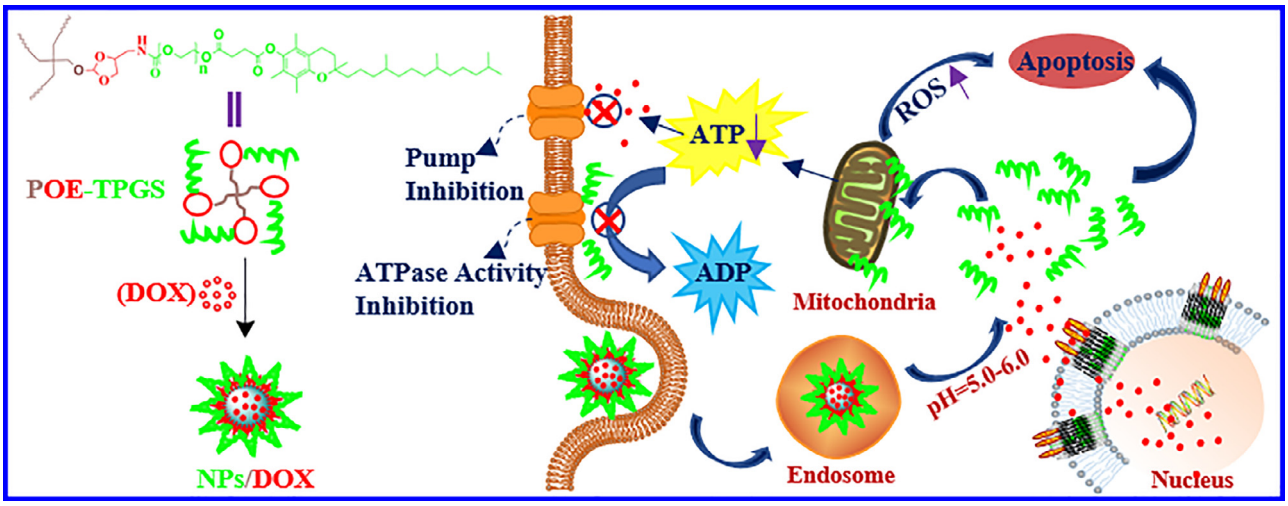


**Scheme 1 – Schematic of pH-sensitive micelles self-assembled from star-shaped TPGS copolymers with ortho ester linkages for enhanced MDR reversal and chemotherapy.**

### 2.4. *Synthesis of star-shaped ortho esters (POE)*

The fluorinated four-arm ortho esters (7.03 mmol, 6.5 g) were dissolved in ethanol and blended with sodium hydroxide aqueous solution (1 mol/l, 50 ml) for 12 h. Afterwards, the mixture was extracted using DCM (50 ml) for three times to yield the product (3.13 g, 82.4%), whose structure was determined by $^{1}$H NMR.

### 2.5. *Synthesis of star-shaped TPGS by ortho ester linkages (POE-TPGS)*

In a nitrogen atmosphere, the mixture of POE (1.14 mmol, 0.62 g), TPGS-active ester (15.0 g), TEA (2.53 ml) and DCM (100 ml) reacted for 24 h and was evaporated by rotary evaporator. The crude product was dissolved in ethanol and dialyzed (5000 Da) against ethanol for 48 h to obtain POE-TPGS (4.94 g, 64.7%), whose structure was determined by $^{1}$H NMR.

### 2.6. *Formation of free and DOX-loaded micelles*

The amphiphilic POE-TPGS could self-assemble into free micelles (NPs) and DOX-loaded micelles (NPs/DOX) via a solvent exchange method, and with the formation of NPs/DOX as an example: In brief, POE-TPGS and DOX with the feeding ratio of 10:1 was dissolved in DMSO and slowly dripped into the stirred PBS (pH 7.4) for 3 h. The mixture was then dialyzed against deionized water for 24 h. Afterwards, NPs/DOX were obtained by centrifugation ($1 \times 10^5$ rpm/min, 15 min).

### 2.7. *Determination of CMC*

The micellar CMC was determined as previously described [42]. Briefly, POE-TPGS-based and TPGS-based micelles with gradient concentrations were exposed to the fluorescence probe (Nile Red) in dark for 24 h, and then measured via a spectrofluorophotometer.

### 2.8. *Determination of DL and EE*

The micellar DOX loading efficiency was determined and calculated referring to the reported reference [42]. Briefly, the prepared NPs/DOX was sequentially lyophilized, weighed, dissolved in DMSO, and determined for UV measurement at 481 nm using Microplate Reader. DL and EE were calculated based on the standard curve of DOX.

### 2.9. *Determination of micellar particle sizes and zeta potentials*

Dynamic light scattering detector (DLS) was applied to determine the micellar sizes and zeta potentials in PBS (pH 7.4 and 5.0) and FBS (pH 7.4), and Scanning Electron Microscope (SEM) was applied to measure the micellar morphology.

### 2.10. *In vitro drug release*

DOX released from NPs/DOX at physiological pH (7.4) and tumoral intracellular pH (5.0) was evaluated by using dialysis bags (MWCO 3500). In brief, NPs/DOX (1 ml) were dialyzed in PBS (5 ml, pH 7.4 or 5.0) at 37 °C, and the dialysate was replaced by the corresponding PBS (5 ml) at the desired time point. Afterwards, The DOX content in each dialysate was determined and calculated via a Microplate Reader at $\lambda_{Excitation}$ 480 nm and $\lambda_{Emission}$ 590 nm and standard curve of DOX.

### 2.11. *In vitro cytotoxicity, cellular uptake and apoptosis*

MCF-7 and MCF-7/ADR cells were applied to evaluate micellar cytotoxicity, cellular uptake and apoptosis as previously described [43]. Briefly, the cells were cultured in 96-well and 6-well plates for 24 h to make cell adherence and proliferation. Afterwards, the cells were co-cultured with DOX formulations for 24 h, 4 and 24 h to determine cytotoxicity,

cellular uptake and apoptosis, respectively. Additionally, NPs were also exposed to two types of cells for 24 h to investigate its proliferation inhibition. The cytotoxicity was measured by MTT assay. The qualitative and quantitative cellular internalization labeled with Hoechst 33,258 or not were determined by confocal laser scanning microscope (CLSM) and flow cytometry respectively. The apoptosis stained using Alexa Fluor® 488 annexin V and PI was confirmed by confocal CLSM.

### 2.12. Measurement of intracellular ROS production

ROS assay kit was used to measure the tumoral intracellular ROS generation. In brief, MCF-7/ADR were seeded on the cover glass in 6-well plates and incubated for 24 h. After co-cultured with NPs (50 μg/ml) for 4 h, washed using cold PBS, exposed to 2,7-dichlorodi-hydrofluorescein diacetate (DCFH-DA) in the dark for 20 min, and washed again using cold PBS, the cells were fixed by 4% of paraformaldehyde for 5 min and detected by a fluorescence inverted microscope.

### 2.13. Measurement of intracellular ATP levels

Briefly, MCF-7/ADR were seeded in 6-well plates and incubated for 24 h. Afterwards, the cells were co-cultured with NPs (0.5, 5.0 and 50.0 μg/ml) for 4 h, washed by cold PBS, solubilized by lysis buffer and centrifugated ($1.2 \times 10^4$ rpm, 10 min) at 4 °C, respectively. The supernatant was measured by ATP assay kit to determine the intracellular ATP levels. Meanwhile, BCA kit was used to measure the protein content in each sample for normalizing the ATP content.

### 2.14. Growth inhibition study of 3-D tumor spheroids in vitro

MCF-7 and MCF-7/ADR multicellular spheroids (MCs) were prepared as described before [43]. Two types of MCs with diameters about 250–300 mm were co-cultured with medium, free DOX and NPs/DOX with the same drug concentration (16 μg/ml) for 7 d, respectively. MCs of each group were photographed by inverted microscope and then measured in diameter every day. The volume of MCs was calculated as follows: $V = (\pi \times a \times b)/6$, where $a$ and $b$ represent the maximum and the minimum diameter of each MCs, respectively.

### 2.15. In vivo biodistribution

DOX-resistant breast cancer model (MCF-7/ADR tumor-bearing nude mice) were applied to evaluate *in vivo* DOX biodistribution as described before [24,44]. Briefly, the mice were treated by free DOX and NPs/DOX at a dose of 5 mg/kg via tail vein injection. Afterwards, the blood samples and major tissues (tumor, liver, heart, lung, kidney and spleen) were surgically obtained from mice at desired time point, whose DOX fluorescence intensity was determined via a Microplate Reader.

### 2.16. In vivo antitumor effect

The tumor regression study was performed using MCF-7/ADR tumor-bearing nude mice as previously described [44]. In brief, the mice were treated by saline, NPs (46.3 mg/kg), free DOX (5 mg/kg), and NPs/DOX (5 mg/kg) via tail vein injection, whose tumor size and weight were measured every day. After 7 d, the tumors were surgically removed, weighed and photographed.

### 2.17. Statistical analysis

Experimental data were presented as the mean ± SD, and the statistical significance was evaluated by SPSS.

## 3. Results and discussion

### 3.1. Preparation and characterization of POE-TPGS and micelles

As shown in Scheme S1, to obtain the pH-sensitive star-shaped TPGS copolymers with ortho ester linkages, pentaerythritol with four hydroxyls was chosen as the starting material, which could react with a pH-triggered ortho ester monomer (TA) via transesterification to yield the FPOE. TPGS was further grafted on the POE by amidation, after trifluoroacetyl groups were removed from FPOE. Notably, whether it was ortho ester monomer or TPGS active-ester, they reacted with pentaerythritol or its derivative at a feeding ratio of 8:1 to ensure a 100% grafting rate. $^1$H NMR and mass spectrum were applied to confirm the successful synthesis of POE-TPGS and its intermediate products (Figs. S1–S4). As displayed in Fig. S2 and S3, the integral area ratio (1:2) of proton peaks between 5.75 ppm (-CH–$O_3$-) in TA and 3.32 ppm (-C-$CH_2$-O-) in pentaerythritol, and the molecular weight of FPOE (924.31) measured by mass spectrum, suggested that all hydroxyls in pentaerythritol were conjugated by ortho ester monomer. Furthermore, as seen in Fig. S4C, the integral areas ratio of proton peaks between 5.75 ppm (-CH–$O_3$-) in POE and 1.96–2.07 ppm (Ph-$CH_3$) in TPGS was 1:3, indicating 100% grafting rate of TPGS on POE.

The amphiphilic star-shaped TPGS with ortho ester linkages could self-assemble into NPs at neutral aqueous solution. As shown in Fig. 1A and S5, the micellar CMC value was determined to be $8.2 \times 10^{-5}$ mg/ml and far lower than that of TPGS-based micelles (0.2 mg/ml), which was possibly attributed to the increased weight of hydrophilic and hydrophobic part for enhancement on intermolecular forces of POE-TPGS via enhanced hydrophobic interaction and $\pi$-$\pi$ stocking, hydrogen bonding interaction and van der Waals force [20,21,31]. The NPs/DOX could be also prepared by self-assembly at PBS (pH 7.4), and their DL and EE were measured to be 10.8% and 74.9% at the mass feeding ratio of 10:1 between the star-shaped TPGS copolymers and DOX. The micellar higher drug loading ability was owing to the enhanced hydrophobic interaction, $\pi$-$\pi$ stocking and hydrogen bonding interaction between hydrophobic vitamin E succinate in the micellar core and DOX [21,28–31]. As shown in Fig. 1B and S6, the average hydrodynamic diameters of NPs/DOX determined

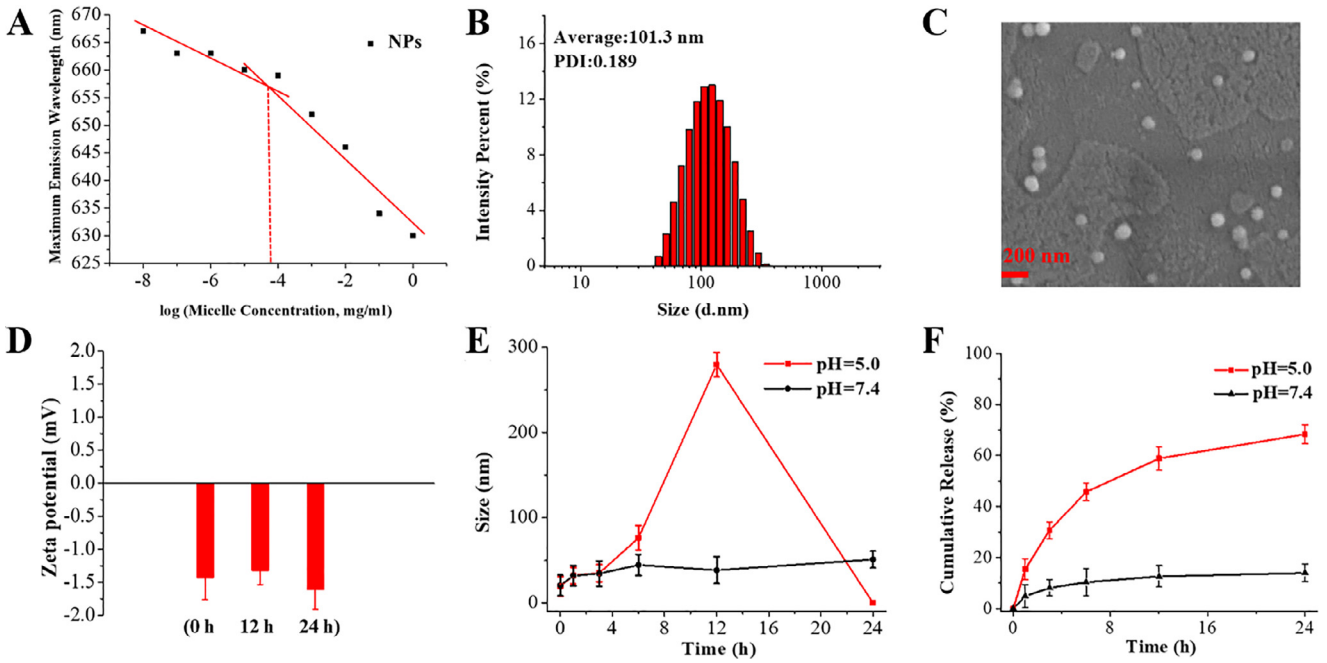


**Fig. 1 – (A) CMC of NPs, (B, C) particle sizes of NPs/DOX, (D) zeta potentials of NPs at pH 7.4, (E) particle size change of NPs, (F) and accumulative DOX release from NPs/DOX.**

by DLS were about 100 nm and could remain unchanged in PBS and FBS for 5d, suggesting the potentially long-term storage and circulation stability [45]. Moreover, as seen in Fig. 1C, NPs/DOX exhibited smaller particle sizes in a drying state observed by SEM. In addition, as displayed in Fig. 1D, the micellar zeta potentials measured by DLS were about −1.5 mV at pH 7.4, further showing their potentially stable blood circulation [46].

### 3.2. *pH sensitivity of POE-TPGS-based micelles*

To evaluate pH sensitivity of the star-shaped TPGS copolymers bearing five-membered ortho ester rings, the micelles were exposed to PBS (pH 7.4 and 5.0) for 24 h. Afterwards, the micellar suspensions were lyophilized and dissolved in $d_6$-DMSO for $^1$H NMR analysis. As shown in Fig. S7, the ortho ester linkages in micelles were not degraded for 24 h at pH 7.4, but fully degraded at pH 5.0. The result showed that POE-TPGS-based micelles could keep stable in blood vessels and be sensitive to tumoral intracellular pH, which might trigger the size alteration and efficient drug release [42]. In addition, as seen in Fig. S8, the degradation of five-membered cyclic ortho ester linkages followed a distinct exocyclic mechanism and the intermediate degradation products might affect drug release via interaction with drugs [47].

### 3.3. *Size transition based on micellar pH sensitivity*

To explore the particle size change at different pH, the micelles were suspended in 1 ml of PBS with different pH values and determined following the time course by DLS. As displayed in Fig. 1E, the micellar particle sizes remained the same for 24 h, which corresponded to the stability of ortho ester linkages revealed by $^1$H NMR (Fig. S7). However, the micellar particle sizes gradually became larger and reached 275 nm from 16.5 nm in 12 h, and then disintegrated at pH 5.0 after 24 h following the full degradation of ortho ester linkages. Such rapid size transition at pH 5.0 could be beneficial for efficient drug release [42,47].

### 3.4. *In vitro drug release*

To evaluate the effect of micellar size transition on drug release, NPs/DOX were put into the dialysis bags and dialyzed against PBS (pH 7.4 and 5.0). As seen in Fig. 1F, the amount of DOX released from NPs/DOX was lower than 10% in 12 h and no longer increased in 24 h at pH 7.4. However, the cumulative amount of DOX release reached about 60% in 12 h, and then continued at a slower but steady pace at pH 5.0. The higher intracellular drug release was beneficial to promote cytotoxicity. Interestingly, drug release behavior corresponded to the behavior of particle size change, suggesting that micellar dynamic size change led to the efficient drug release. In addition, DOX in NPs/DOX did not fully release, although the ortho ester linkages had been fully degraded at pH 5.0 after 24 h. It might be because of the hydrophobic interaction, $\pi$-$\pi$ stocking and hydrogen bonding interactions between the intermediate degradation products and DOX as shown in Fig. S8, which delayed the drug release.

### 3.5. *Micellar cytotoxicity, cellular uptake and apoptosis*

MCF-7 and MCF-7/ADR were applied to evaluate the effect of pH-sensitive micelles self-assembled from the orthoester-linked star-shaped TPGS copolymers on pharmacological activity. The NPs as negative control were also exposed to the

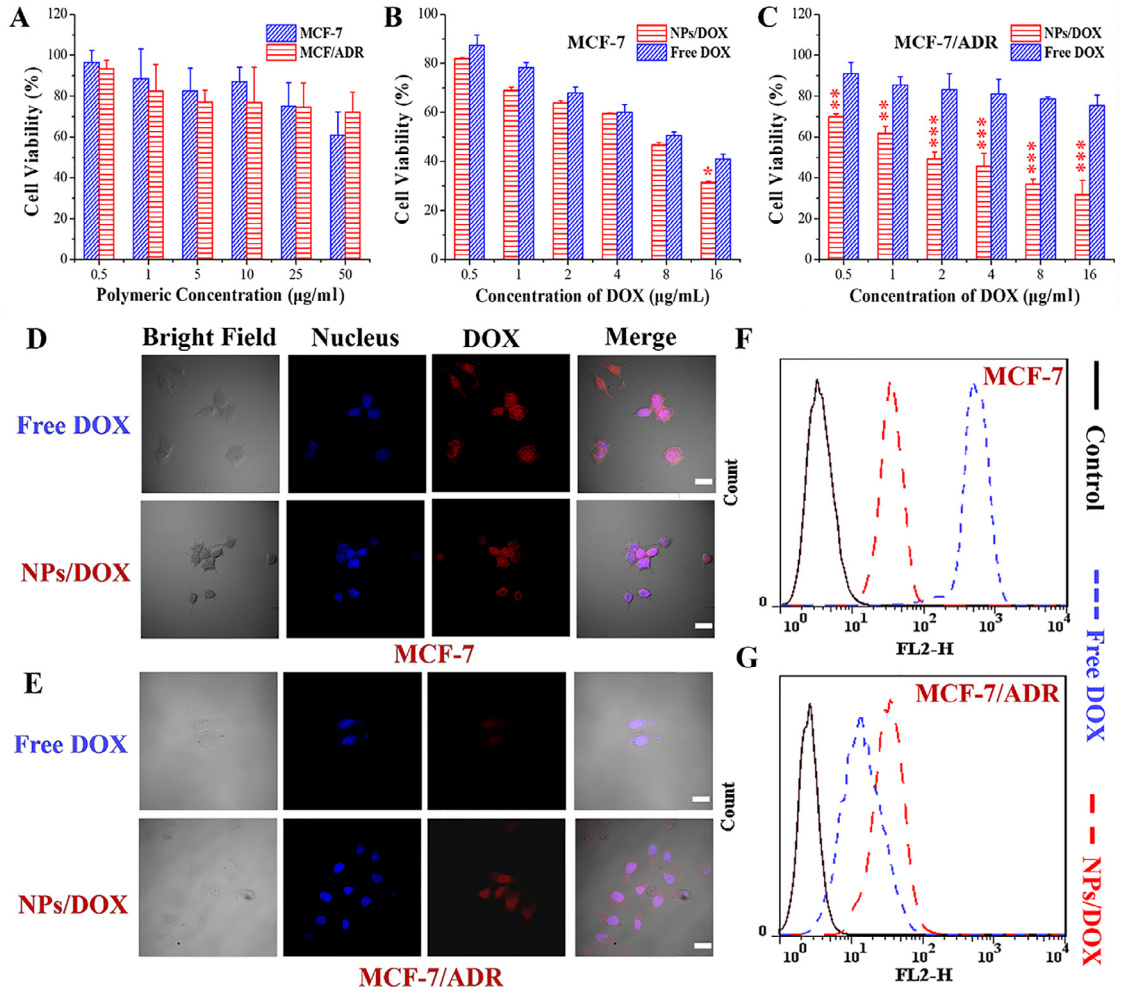


**Fig. 2 – *In vitro* dose-dependent cytotoxicity of free micelles (A) and various DOX formulations (B, C) in MCF-7 and MCF-7/ADR for 24 h determined by MTT assay (* represents $P < 0.05$, ** represents $P < 0.01$ and *** represents $P < 0.001$), and cellular uptake (D-G) of various DOX formulations (16 μg/ml) for 4 h measured by confocal fluorescence microscopy and flow cytometry respectively; Scale bar = 10 μm.**

two types of tumor cells to measure the cytotoxicity of TPGS. As shown in Fig. 2A, when the micellar concentration was higher than 1 μg/ml, the NPs could restrain the proliferation of both MCF-7 and MCF-7/ADR via the mechanisms like mitochondrial destabilization, downregulation of anti-apoptotic proteins and DNA damage [15], once TPGS was released from the NPs at tumoral intracellular pH. As seen in Fig. 2B and 2C, the NPs/DOX achieved the more significant cytotoxicity than free DOX for both of MCF-7 and MCF-7/ADR. Notably, free DOX showed an apparently weak ability to inhibit the proliferation of MCF-7/ADR compared to MCF-7, but NPs/DOX displayed the similar cytotoxicity to two types of tumor cells. Furthermore, as shown in Fig. 2D-2G, the uptake of NPs/DOX was weaker than free DOX by MCF-7, but stronger by MCF-7/ADR via qualitative and quantitative analysis using CLSM and flow cytometry, respectively. These results suggested that NPs/DOX based on pH-sensitive star-shaped TPGS copolymers could efficiently reverse ADR, remain cellular uptake and improve the cell-killing ability through synergistic effect of TPGS and DOX. In addition, two types of tumor cells were co-cultured with DOX formulations (16 μg/ml) for 24 h and stained using Alexa Fluor® 488 annexin V and PI. As seen in Fig. 3A, the apoptosis rate of MCF-7 was 49.5% and 68.2% and that of MCF-7/ADR was 11.6% and 63.4% induced by free DOX and NPs/DOX, respectively. The result suggested that the cell death was mainly caused by apoptosis, and NPs/DOX showed the similar pro-apoptotic abilities for MCF-7 and MCF-7/ADR owing to the MDR reversal, but free DOX exhibited obviously lower pro-apoptotic abilities for MCF-7/ADR than MCF-7, due to the MDR in MCF-7/ADR. Moreover, NPs/DOX had the stronger ability to promote apoptosis than free DOX for MCF-7/ADR based on ADR reversal and synergistic effect of TPGS and DOX [43].

### 3.6. *ROS generation in MCF-7/ADR*

To further demonstrate whether the cause of cytotoxicity by NPs was related to ROS generation, MCF-7/ADR were co-cultured with NPs for 4 h and determined by ROS assay kit. Intracellular green fluorescence represented ROS generation

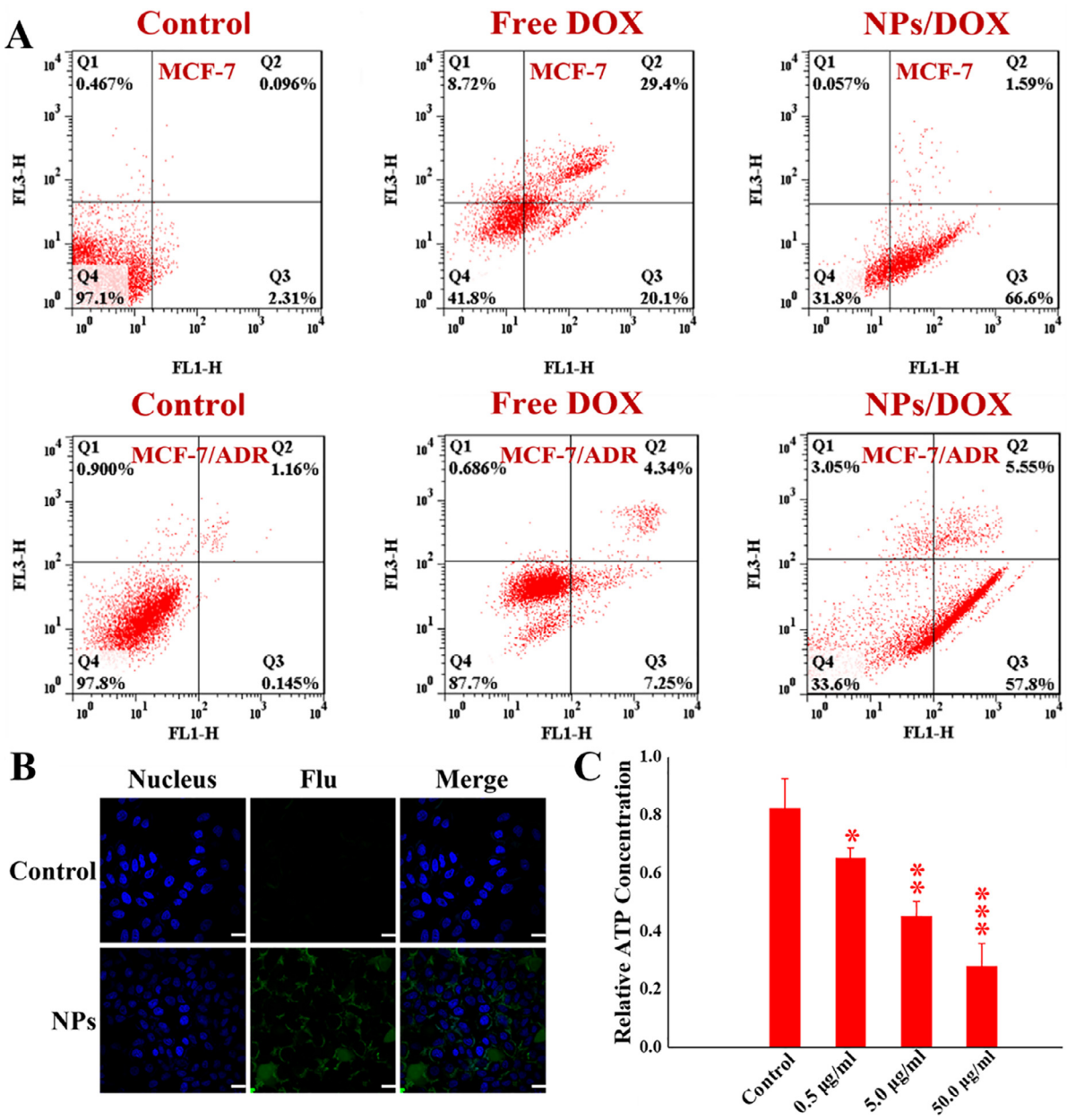


**Fig. 3 – Apoptosis of MCF-7 and MCF-7/ADR induced by various DOX formulations (16 μg/ml) for 24 h confirmed by flow cytometry (A), and ROS generation (B) and intracellular ATP content (C) in MCF-7/ADR treated by control and free micelles for 4 h, respectively (* represents $P < 0.05$, ** represents $P < 0.01$ and *** represents $P < 0.001$); Scale bar = 10 μm.**

[44]. As seen in Fig. 3B, compared with control group, large amounts of green fluorescence signals were found in MCF-7/ADR, indicating that NPs self-assembled from amphiphilic pH-sensitive star-shaped TPGS copolymers could induce cells to produce ROS, possibly owing to the mitochondria impairment by TPGS in micelles [15], once the micelles hydrolyzed and yielded TPGS under intracellular low pH.

### 3.7. *Downregulation of intracellular ATP levels*

As well known, P-gp belongs to the ATP-binding cassette (ABC) family, so the intracellular ATP levels directly determine the activity of drug efflux [3,7,8]. As displayed in Fig. 3C, in comparison with the control, NPs self-assembled from pH-sensitive star-shaped TPGS copolymers could significantly decrease intracellular ATP levels of MCF-7/ADR as the micellar concentration increased, suggesting that one of the mechanisms by which the micelles reverse MDR was inhibition of drug efflux by down-regulating intracellular ATP levels.

### 3.8. *Growth inhibition of MCF-7 and MCF-7/ADR MCs*

To further explore the effect of micelle self-assembled from the ortho ester-linked star-shaped TPGS copolymers on tumor growth inhibition, the tumoral multicellular spheroids based

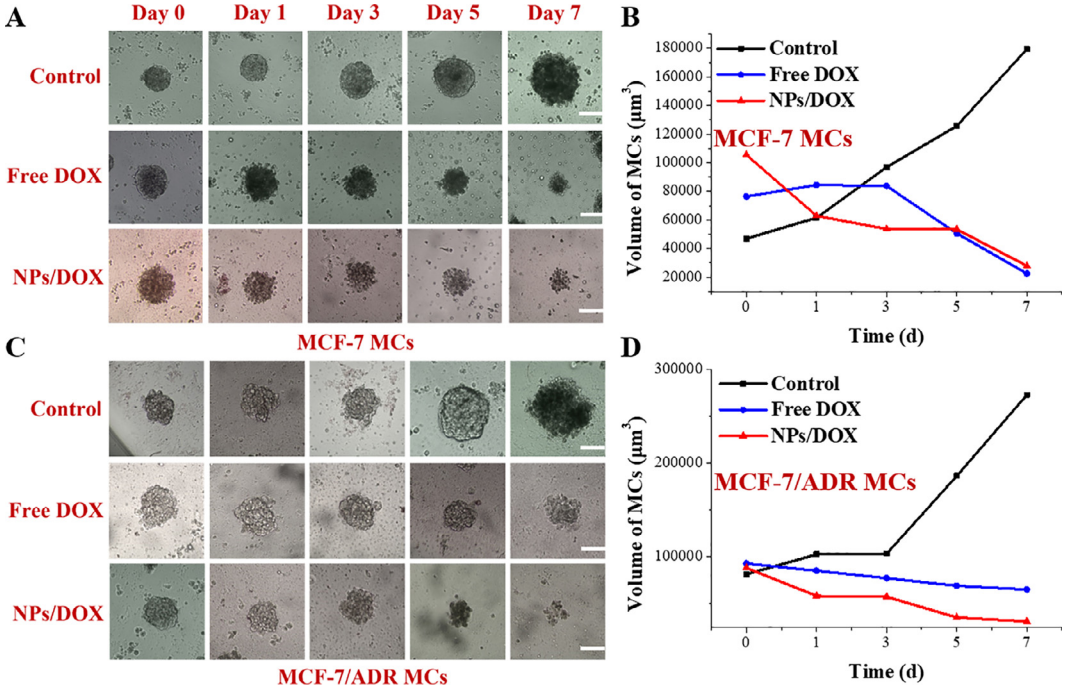


**Fig. 4 – Growth inhibition of MCF-7 MCs (A, B) and MCF-7/ADR MCs (C, D) by various DOX formulations for 7 d; Scale bar = 300 μm.**

on MCF-7 and MCF-7/ADR, representing *in vitro* tumor model without blood vessels, were successfully prepared according to the previous literature [43]. NPs/DOX and free DOX with same drug concentration (16 μg/ml) were exposed to the two types of MCs with diameters about 250–300 μm for 7 d, and the diameters of MCs were observed and measured each day using the inverted microscope. As revealed in Fig. 4, MCs treated by medium exhibited the significant tumor growth and gradually became pyknotic following the time course, owing to the tumoral cellular interactions and extracellular matrix secretion [48]. Contrarily, MCs treated by DOX formulations gradually became small and incompact. Notably, free DOX displayed the stronger growth inhibition of MCF-7 MCs than that of MCF-7/ADR MCs, but NPs/DOX showed similar tumor inhibition in two types of MCs. Furthermore, NPs/DOX exhibited similar tumor inhibition ability with free DOX for MCF-7 MCs, but stronger for MCF-7/ADR. Additionally, the two types of MCs treated by NPs/DOX showed looser tumor structure in comparison with that treated by free DOX. These results suggested that pH-sensitive NPs/DOX based on ortho ester-linked star-shaped TPGS copolymers had stronger growth inhibition for MDR tumor via the MDR reversal and pH sensitivity for improved cellular internalization, drug release and cytotoxicity.

### 3.9. *Pharmacokinetics and in vivo biodistribution*

To investigate the pharmacokinetics and *in vivo* biodistribution of NPs/DOX, the nude mice bearing MCF-7/ADR xenograft tumors were given a single injection of free DOX and NPs/DOX by tail vein injection at a dose of 5 mg/kg DOX. As displayed in Fig. 5, the results clearly showed the diversity of DOX content in each tissue. By comparison with free DOX, on one hand, NPs/DOX exhibited higher blood and tumor drug concentrations at each time point, suggesting their blood circulation stability and enhanced tumor accumulation owing to PEG-coating, EPR effect, targeted drug release and MDR reversal, respectively [3,5,13,32–34]. On the other hand, NPs/DOX exhibited lower drug concentrations in heart, spleen, lung, and kidney tissues, indicating their reduced side effect [5], but higher in liver tissue, which was possibly because NPs/DOX in the metabolic cycle *in vivo* might be transformed into smaller particles, and most of particles were cleared by the liver tissue [33,49].

### 3.10. *In vivo antitumor effects*

*In vivo* anti-tumor efficiency of various formulations was further evaluated in MCF-7/ADR tumor-bearing nude mice. Saline, NPs, free DOX and NPs/DOX were once administrated by tail vein injection after tumor inoculation. As seen in Fig. 6A, 6C and 6D, free DOX exhibited little tumor inhibition, possibly due to MDR and low drug accumulation at tumor site [1–3]. Interestingly, NPs showed similar inhibitory effect with free DOX via EPR effect and cytotoxicity of TPGS [11–14]. Compared with free DOX and NPs groups, NPs/DOX group displayed the smaller tumor size and weight via the stable blood circulation, enhanced drug aggregation at tumor site, MDR reversal, effective pH-triggered drug release, and synergistic effect of DOX and TPGS. In addition, as shown in Fig. 6B, compared to other groups, free DOX made mice lose body weight at Day 2, further indicating their apparent adverse effects on normal tissues [48].

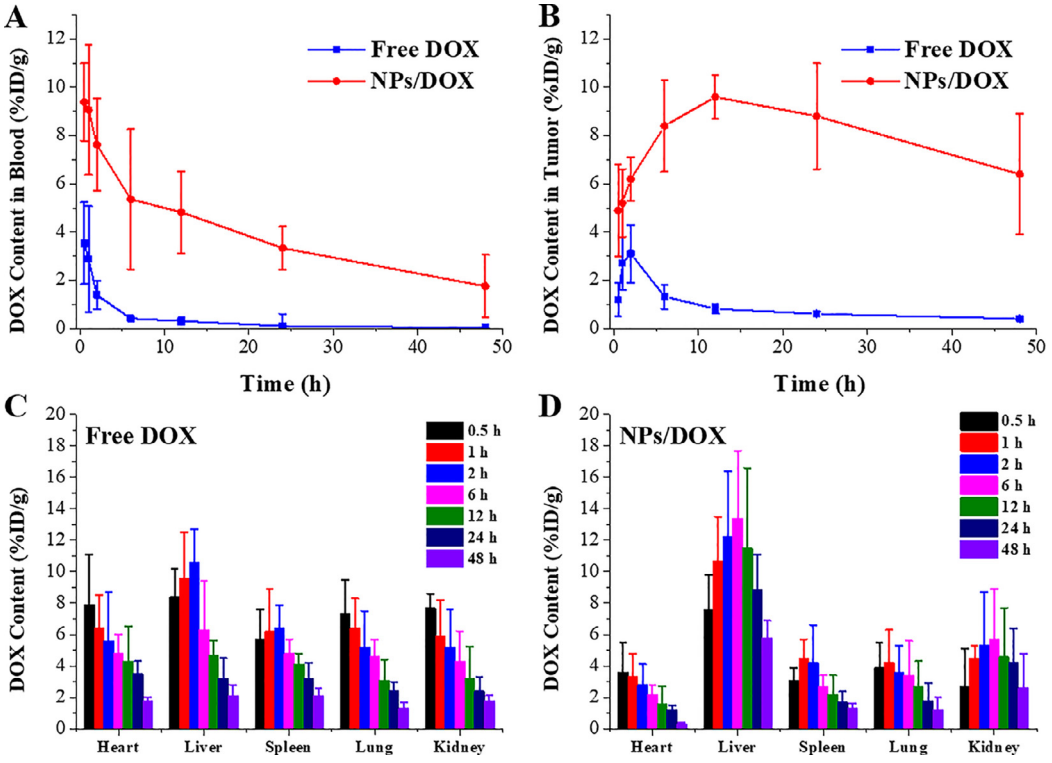


**Fig. 5 – *In vivo* distributions of DOX in MCF-7/ADR tumor-bearing nude mice. Pharmacokinetic behaviors of DOX after intravenous injection of free DOX and NPs/DOX in blood (A) and tumor tissue (B), and biodistribution of free DOX (C) and NPs/DOX (D) in normal tissues.**

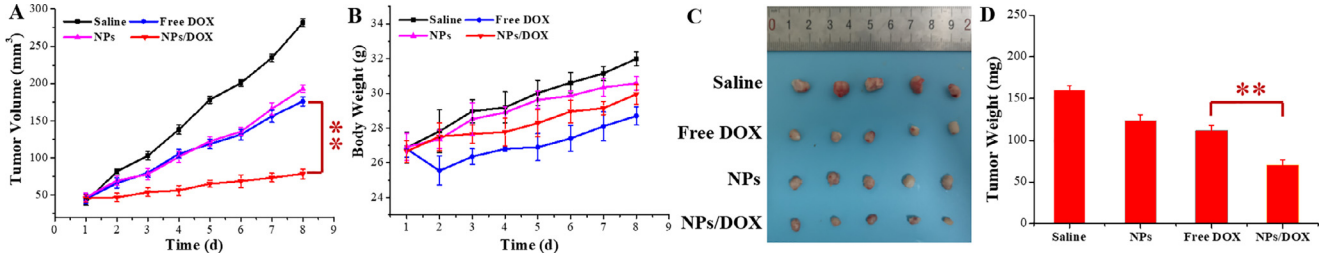


**Fig. 6 – *In vivo* antitumor efficacy study. Changes in tumor volume (A) and body weight (B). Tumor image (C) and weight (D) at the end time point of the treatment. (**represents $P < 0.01$).**

## 4. Conclusion

In summary, the pH-sensitive star-shaped copolymers with ortho ester linkages were successfully constructed via a facile method, and could self-assemble into free and DOX-loaded micelles. The micelles exhibited lower CMC and higher drug loading compared to TPGS-based micelles. Moreover, the micelles showed suitable drug-loaded particle sizes (101.3 nm), negative zeta potential (−1.5 mV) at pH 7.4, long-term stability in PBS and FBS, efficient drug release at pH 5.0, and enhanced cellular uptake, apoptosis, and cytotoxicity for MCF-7/ADR, via intracellular pH sensitivity, MDR reversal and synergistic effect of DOX and TPGS. Additionally, the micelles could significantly inhibit the growth of *in vitro* MCF-7/ADR MCs and *in vivo* MCF-7/ADR tumors. Therefore, pH-sensitive micelles self-assembled from star-shaped TPGS copolymers with ortho ester linkages have great potential to be used for reversing MDR in clinical cancer therapy.

## Conflicts of interest

The authors report no conflicts of interest. The authors alone are responsible for the content and writing of this article.

## Acknowledgements

This work is financially supported by the National Natural Science Foundation of China (No. 51803001), the Research Foundation of Education Department of Anhui Province of

China (No. KJ2018ZD003 and KJ2018A0006), and the Academic and Technology Introduction Project of Anhui University (AU02303203).

## Supplementary materials

Supplementary material associated with this article can be found, in the online version, at doi:10.1016/j.ajps.2021.01.002.

REFERENCES

[1] Tóth S, Szepesi Á, Tran-Nguyen VK, Sarkadi B, Német K, Falson P, et al. Synthesis and anticancer cytotoxicity of azaaurones overcoming multidrug resistance. Molecules 2020;25(3):764.
[2] Tan W, Zhong Z, Carney RP, Men Y, Li J, Pan T, Wang Y. Deciphering the metabolic role of AMPK in cancer multi-drug resistance. Semin Cancer Biol 2019;56:56–71.
[3] Wu Q, Yang Z, Nie Y, Shi Y, Fan D. Multi-drug resistance in cancer chemotherapeutics: mechanisms and lab approaches. Cancer Lett 2014;347(2):159–66.
[4] Chen Q, Yang Y, Lin X, Ma W, Chen G, Li W, Wang X, Yu Z. Platinum(iv) prodrugs with long lipid chains for drug delivery and overcoming cisplatin resistance. Chem Commun 2018;54:5369–72.
[5] Yang C, Xing L, Chang X, Zhou T, Bi Y, Yu Z, Zhang Z, Jiang H. Synergistic platinum(II) prodrug nanoparticles for enhanced breast cancer therapy. Mol Pharm 2020;17(4):1300–9.
[6] Sun Y, Ma W, Yang Y, He M, Li A, Bai L, Yu B, Yu Z. Cancer nanotechnology: enhancing tumor cell response to chemotherapy for hepatocellular carcinoma therapy. Asian J Pharm Sci 2019;14(6):581–94.
[7] Chen Z, Shi T, Zhang L, Zhu P, Deng M, Huang C, Hu T, Liang L, Li J. Mammalian drug efflux transporters of the ATP binding cassette (ABC) family in multidrug resistance: a review of the past decade. Cancer Lett 2016;370(1):153–64.
[8] Kathawala RJ, Gupta P, Ashby Jr CR, Chen Z. The modulation of ABC transporter-mediated multidrug resistance in cancer: a review of the past decade. Drug Resist Update 2015;18:1–17.
[9] Callaghan R, Luk F, Bebawy M. Inhibition of the multidrug resistance P-glycoprotein: time for a change of strategy? Drug Metab Dispos 2014;42(4):623–31.
[10] Sosnik A. Reversal of multidrug resistance by the inhibition of ATP-binding cassette pumps employing “Generally Recognized As Safe” (GRAS) nanopharmaceuticals: a review. Adv Drug Deliv Rev 2013;65(13–14):1828–51.
[11] Zhang Z, Tan S, Feng SS. Vitamin E TPGS as a molecular biomaterial for drug delivery. Biomaterials 2012;33(19):4889–906.
[12] Choudhury H, Gorain B, Pandey M, Kumbhar SA, Tekade RK, Lyer AK, Kesharwani P. Recent advances in TPGS-based nanoparticles of docetaxel for improved chemotherapy. Int J Pharm 2017;529(1–2):506–22.
[13] Zhang Z, Mei L, Feng SS. Vitamin E D-$\alpha$-tocopheryl polyethylene glycol 1000 succinate-based nanomedicine. Nanomedicine 2012;7(11):1645–7.
[14] Pham CV, Cho CW. Application of D-$\alpha$-tocopheryl polyethylene glycol 1000 succinate (TPGS) in transdermal and topical drug delivery systems (TDDS). J Pharm Investig 2017;47(2):111–21.
[15] Yang C, Wu T, Qi Y, Zhang Z. Recent advances in the application of vitamin E TPGS for drug delivery. Theranostics 2018;8(2):464–85.
[16] Tuguntaev RG, Chen S, Eltahan AS, Mozhi A, Jin S, Zhang J, Li C, Wang PC, Liang XJ. P-gp inhibition and mitochondrial impairment by dual-functional nanostructure based on vitamin E derivatives to overcome multidrug resistance. ACS Appl Mater Interfaces 2017;9(20):16900–12.
[17] Jin Y, Wu Z, Li C, Zhou W, Shaw JP, Baguley BC, Liu J, Zhang W. Optimization of weight ratio for DSPE-PEG/TPGS hybrid micelles to improve drug retention and tumor penetration. Pharm Res 2018;35(1):13.
[18] Yang L, Zhang Z, Hou J, Jin X, Ke Z, Liu D, Du M, Jia X, Lv H. Targeted delivery of ginsenoside compound K using TPGS/PEG-PCL mixed micelles for effective treatment of lung cancer. Int J Nanomedicine 2017;12:7653–67.
[19] Wang Z, Sau S, Alsaab HO, Lyer AK. CD44 directed nanomicellar payload delivery platform for selective anticancer effect and tumor specific imaging of triple negative breast cancer. Nanomed Nanotechnol 2018;14(4):1441–54.
[20] Jungnickel C, Łuczak J, Ranke J, Fernández JF, Müller A, Thöming J. Micelle formation of imidazolium ionic liquids in aqueous solution. Colloid Surf A 2018;316(1–3):278–84.
[21] Li Y, Yang L. Driving forces for drug loading in drug carriers. J Microencapsul 2015;32(3):255–72.
[22] Khare V, Sakarchi WA, Gupta PN, Curtis ADM, Hoskins C. Synthesis and characterization of TPGS-gemcitabine prodrug micelles for pancreatic cancer therapy. RSC Adv 2016;6(65):60126–37.
[23] Qiao H, Zhu Z, Fang D, Sun Y, Kang C, Di L. Redox-triggered mitoxantrone prodrug micelles for overcoming multidrug-resistant breast cancer. J Drug Target 2018;26(1):75–85.
[24] Bao Y, Yin M, Hu X, Zhuang X, Sun Y, Guo Y, Tan S, Zhang Z. A safe, simple and efficient doxorubicin prodrug hybrid micelle for overcoming tumor multidrug resistance and targeting delivery. J Control Release 2016;235:182–94.
[25] de Melo-Diogo D, Gaspar VM, Costa EC, Moreira AF, Oppolzer D, Gallardo E, Correia LJ. Combinatorial delivery of Crizotinib–Palbociclib–Sildenafil using TPGS-PLA micelles for improved cancer treatment. Eur J Pharm Biopharm 2014;88(3):718–29.
[26] Singh RP, Sharma G, Agrawal P, Pandey BL, Koch B, Muthu MS. Transferrin receptor targeted PLA-TPGS micelles improved efficacy and safety in docetaxel delivery. Int J Biol Macromol 2016;83:335–44.
[27] Zhao D, Zhang H, Yang S, He W, Luan Y. Redox-sensitive mPEG-SS-PTX/TPGS mixed micelles: an efficient drug delivery system for overcoming multidrug resistance. Int J Pharm 2016;515(1–2):281–92.
[28] Zeng X, Tao W, Wang Z, Zhang X, Zhu H, Wu Y, Gao Y, Liu K, Jiang Y, Huang L, Mei L, Feng SS. Docetaxel-loaded nanoparticles of dendritic amphiphilic block copolymer H40-PLA-b-TPGS for cancer treatment. Part Part Syst Char 2015;32(1):112–22.
[29] Wang Y, Grayson SM. Approaches for the preparation of non-linear amphiphilic polymers and their applications to drug delivery. Adv Drug Deliv Rev 2012;64(9):852–65.
[30] Maglio G, Nese G, Nuzzo M, Palumbo R. Synthesis and characterization of star-shaped diblock poly($\varepsilon$-caprolactone)/poly(ethylene oxide) copolymers. Macromol Rapid Commun 2004;25(12):1139–44.
[31] Wang S, Zhou Y, Zhuang B, Zheng P, Chen H, Zhang T, Hu H, Huang D. Star-shaped amphiphilic block polyurethane with pentaerythritol core for a hydrophobic drug delivery carrier. Polym Int 2016;65(5):551–8.
[32] Stapleton S, Jaffray D, Milosevic M. Radiation effects on the tumor microenvironment: implications for nanomedicine delivery. Adv Drug Deliv Rev 2017;109:119–30.
[33] Chauhan VP, Jain RK. Strategies for advancing cancer nanomedicine. Nat Mater 2013;12(11):958–62.

[34] Thakkar S, Sharma D, Kalia K, Tekade RK. Tumor microenvironment targeted nanotherapeutics for cancer therapy and diagnosis: a review. Acta Biomater 2020;101:43–68.
[35] Thews O, Riemann A. Tumor pH and metastasis: a malignant process beyond hypoxia. Cancer Metastasis Rev 2019;38(1–2):113–29.
[36] Xing Y, Xu Z, Liu T, Shi L, Kohane D, Guo S. Synthesis of poly (acyclic Orthoesters): acid-sensitive biomaterials for enhancing immune responses of protein vaccine. Angew Chem Int Ed 2020;59(18):7235–9.
[37] Mura S, Nicolas J, Couvreur P. Stimuli-responsive nanocarriers for drug delivery. Nat Mater 2013;12(11):991–1003.
[38] Wang C, Ge Q, Ting D, Nguyen D, Shen H, Chen J, Eisen HN, Heller J, Langer R, Putnam D. Molecularly engineered poly (ortho ester) microspheres for enhanced delivery of DNA vaccines. Nat Mater 2004;3(3):190–6.
[39] Kaur J, Aggarwal G, Singh G, Rana AC. Improvement of drug solubility using solid dispersion. Int J Pharm Pharm Sci 2012;4(2):47–53.
[40] Yan G, Huang Y, Li D, Xu Y, Wang J, Wang X, Tang R. Sequentially dynamic polymeric micelles with detachable PEGylation for enhanced chemotherapeutic efficacy. Eur J Pharm Biopharm 2019;145:54–64.
[41] Yu M, Zhang L, Wang J, Tang R, Yan G, Cao Z, Wang X. Acid-labile poly (ortho ester amino alcohols) by ring-opening polymerization for controlled DNA release and improved serum tolerance. Polymer 2016;96:146–55.
[42] Yan G, Wang J, Hu L, Wang X, Yang G, Fu S, Cheng X, Zhang P, Tang R. Stepwise targeted drug delivery to liver cancer cells for enhanced therapeutic efficacy by galactose-grafted, ultra-pH-sensitive micelles. Acta Biomater 2017;51:363–73.
[43] Sun M, Wang X, Cheng X, He L, Yan G, Tang R. TPGS-functionalized and ortho ester-crosslinked dextran nanogels for enhanced cytotoxicity on multidrug resistant tumor cells. Carbohydr Polym 2018;198:142–54.
[44] Cheng X, Lv X, Xu J, Zheng Y, Wang X, Tang R. Pluronic micelles with suppressing doxorubicin efflux and detoxification for efficiently reversing breast cancer resistance. Eur J Pharm Sci 2020;146:105275.
[45] Sun Q, Sun X, Ma X, Zhou Z, Jin E, Zhang B, Shen Y, Kirk EV, Murdoch W, Lott J, Lodge T, Radosz M, Zhao Y. Integration of nanoassembly functions for an effective delivery cascade for cancer drugs. Adv Mater 2014;26(45):7615–21.
[46] Yang Y, Yuan SX, Zhao LH, Wang C, Ni JS, Wang ZG, Lin C, Wu MC, Zhou WP. Ligand-directed stearic acid grafted chitosan micelles to increase therapeutic efficacy in hepatic cancer. Mol Pharm 2015;12(2):644–52.
[47] Yan G, Wang J, Zhang P, Hu L, Wang X, Yang G, Fu S, Cheng X, Tang R. Tunable dynamic fluorinated poly (orthoester)-based drug carriers for greatly enhanced chemotherapeutic efficacy. Polym Chem 2017;8(13):2063–73.
[48] Wang X, Yang C, Zhang Y, Zhen X, Wu W, Jiang X. Delivery of platinum(IV) drug to subcutaneous tumor and lung metastasis using bradykinin-potentiating peptide-decorated chitosan nanoparticles. Biomaterials 2014;35(24):6439–53.
[49] Minchin R. Sizing up targets with nanoparticles. Nat Nanotechnol 2008;3(1):12–13.